Probing anodic oxidation kinetics and nanoscale heterogeneity within TiO_2 films by Conductive Atomic Force Microscopy and combined techniques

M.V. Diamanti [a,*], T. Souier [b], M. Stefancich [b], M. Chiesa [b], M.P. Pedeferri [a]

[a] *Politecnico di Milano, Department of Chemistry, Materials and Chemical Engineering "Giulio Natta", Milan, Italy*
[b] *Laboratory of Energy and Nanosciences, Masdar Institute of Science and Technology, Abu Dhabi, United Arab Emirates*

Article history:
Received 11 November 2013
Received in revised form 19 February 2014
Accepted 19 February 2014
Available online 3 March 2014

1. Introduction

Advanced applications of titanium dioxide, for instance in the production of optical coatings and in electronics, generally rely on the production of an oxide film few nanometers or tens of nanometers thick, and necessitate a precise control of oxide characteristics [1–4]. This in turn requires a suitable technique, or set of techniques, both to produce and to characterize the desired nanoscale oxides. Specifically concerning oxide production, anodic oxidation is a versatile process that allows to grow an oxide layer with thickness, structure, color, and electrical properties controlled by process parameters imposed–electrolyte composition, temperature, current density, and cell voltage [5–7].

Still, a deeper understanding of oxide properties is vital to open the way to engineered applications of thin nanostructured TiO_2 films, which also show peculiar electrical performances whose features strictly depend on oxide thickness and structure. Among these, the latest application–still at an early stage of development–is the production of memristive devices, i.e., passive resistive circuit elements where resistance is a function of the current that has traveled through the device in the past [8–10]. The first two-terminal memristive device ever realized consisted of a 5 nm thick, non-stoichiometric titanium dioxide film, whose defective nature was responsible for the non-linear behavior; thin anodic TiO_2 films also present this peculiarity, and are therefore suitable to create such devices [11–13]. Two switching mechanisms are generally considered: a mobile ionic mechanism and a filament based mechanism. In the former case, ionic imbalance can be obtained by introducing a vacancy or donor concentration gradient, or through multi-layered structures with different charge concentrations [8]. In the filament based mechanism, resistive states switch to low resistive states through the formation and disconnection of a local conduction path, generally represented by changes of crystalline phase: in this case, the process is never completely reversible [13–15]. Memristive properties of TiO_2 films can be traced back to both mechanisms: in the former case, the alignment of stoichiometric defects due to the presence of Ti^{2+} and Ti^{3+} ions (i.e., oxygen vacancies) caused by the application of an electric field induces the switch; in the latter, the formation and disruption of crystalline domains of Ti_nO_{2n-1} (Magnéli phases) was proved to cause the switching behavior observed [16]. It is therefore clear how an optimal control of oxide composition and crystal structure

* Corresponding author. Tel.: +39223993137; fax: +39223993180.
E-mail address: mariavittoria.diamanti@polimi.it (M.V. Diamanti).

becomes vital to tune oxide properties, together with oxide thickness, as memristance is inversely proportional to the square of the oxide thickness [8,17].

In this respect, the appearing of interference colors can be exploited as a reliable and simple indirect measurement of oxide thickness. In fact, thin amorphous films produce the appearance of a color on the surface of titanium, owing to visible light interference occurring between part of the radiation reflected by the film outer surface and the remaining part refracted through the film, and subsequently reflected by the titanium surface underneath. The hue generated is therefore determined by oxide thickness, with colors ranging from yellow (30 to 40 nm), to purple, blue, and then violet, green and pink at growing oxide thickness, when the oxide is thick enough to produce multiple interference peaks in the visible light range [18–20]. Unfortunately, visible light interference only appears at oxide thickness higher than 30-40 nm: below this threshold, a very restricted number of techniques can be taken into account, among which coulometric measurements can represent a valuable source of information by deriving oxide thickness from Faraday's law (Eq. 1) [21]:

$$\delta = \Delta m/\rho \cdot A = M \cdot Q/(z \cdot F \cdot \rho \cdot A) \quad (1)$$

where δ = oxide thickness, Δm = oxide mass produced in the reaction, A = anodized area, ρ = oxide density and M = molecular weight, Q = charge circulating in the system provided by titanium oxidation, z = titanium valence and F = Faraday's constant.

Coulometric measurements show, however, limitations in the evaluation of oxide thickness: in fact, Faraday's law can be effectively applied only if (i) a precise value for oxide density, ρ, is known and (ii) the anodizing process is 100% efficient, meaning no current is consumed by concurrent reactions. Yet, anodizing efficiency is affected by the parasitic reaction of oxygen evolution, which is incentivized by the presence of crystal structures in the oxide that promote electric conductivity [5]. To verify this aspect, the most typical techniques–such as X-ray diffraction and Raman spectroscopy–involve an exceedingly wide volume of material, thus showing poor sensitivity to nanocrystalline domains embedded in few tens of nanometers thick oxides.

The critical aspects presented highlight the need for a set of experimental techniques capable of providing precise information on both structure and thickness of anodic oxides. Given these premises, spectrophotometry and coulometric measurements were used to indirectly evaluate oxide thickness. These methods were used in combination with Conductive Atomic Force Microscopy (C-AFM), which is the ideal technique to investigate with high spatial resolution the electrical properties of thin oxide layers, providing information on the oxide nanostructure and identifying the presence of heterogeneities such as thickness variations [22], stoichiometric defects [23], amorphous and crystalline domains [24] across the surface. Such technique has already proven its value in the identification and characterization of memristive domains [25–27]. This multidisciplinary approach allowed to address issues left open by single techniques through the combination of optical, electrochemical and electrical measurements, providing a more complete vision of oxide properties at both the macro and the nanoscale.

2. Experimental

Commercial purity titanium specimens, grade 2 in ASTM classification, were anodized in diluted sulfuric acid (0.5 M) in galvanostatic mode by allowing cell voltage to reach values ranging from 3 V to 90 V. Particular attention was paid to oxides produced at the lowest voltages (3 to 10 V). Prior to anodizing, specimens were degreased with acetone and subjected to acid pickling in a HF/HNO_3 mixture (5% and 20% by weight, respectively) to remove contaminations and pre-existing oxides from the metal surface. Cell voltage was measured as anode-to-cathode potential, being the anode the specimen to be anodized and the cathode an activated titanium net, both positioned in a 1 l beaker and immersed in the anodizing electrolyte. Different current densities were applied, ranging from 5 mA/cm^2 to 40 mA/cm^2. The total current circulated through the circuit was measured by means of a data logger.

At the end of the anodizing process, surface reflectance spectra were measured by means of a portable reflectance spectrophotometer operating in the range 360 nm–740 nm. Interference spectra produced by transparent thin films present a sinusoidal trend, with peaks and valleys associated to wavelengths where constructive or destructive interference occurs, respectively, as more thoroughly described in a previous work [28]. The position of reflectance peaks and valleys was then translated into oxide thickness by applying Eq. 2:

$$n_{TiO_2} \cdot \lambda = 2\delta \cdot \sin\theta \quad (2)$$

where n_{TiO2} = oxide refractive index, λ = radiation wavelength giving interference, δ = oxide thickness, θ = incident angle of light. Due to uncertainties in oxide crystal structure, which would modify the oxide refractive index, a thickness range was considered rather than single values, with two boundary values for each cell voltage represented by thickness calculated with a maximum refractive index (n_c = 2.5 at 632.8 nm) typical of crystalline oxides, and a minimum refractive index (n_a = 2.2 at 632.8 nm) typical of amorphous oxides [19,29,30].

Specimens anodized with low voltage were then subjected to C-AFM measurements, performed with MFP-3D AFM from Asylum Research equipped with dual gain ORCA module: the first gain range, consisting of a resistance of 1 MΩ, allowed current measurements from 1 pA to 10 nA, while the second gain range presents a 3 orders of magnitude higher resistance (GΩ), consequently allowing current measurements in a range 3 orders of magnitude higher (from 10 nA to 10 μA). A more detailed description of the dual gain C-AFM setup can be found in previous work [31]. A highly doped boron-diamond tip (tip radius 80 nm [32], spring constant of 40 N/m) from Nanosensors was used to probe, with nanometric resolution, the electronic properties of the oxide layer [23,33]. The softwares Gwyddion and WSxM were used for C-AFM data processing [34,35]. From such measurements, roughness information was also derived: also in this case the software Gwyddion was employed to quantify the maximum and average roughness, and to estimate the ratio between specific surface area and projected area.

Table 1
Roughness values extracted from multiple AFM scans of anodized specimens.

	Scan size (μm^2)	R_a (nm)	h_{max} (nm)	ΔA % ($A_{specific}$ vs $A_{projected}$)
3 V	100	86	685	3.8
6 V	100	122	914	6.4
9 V	100	68	665	2.6
3 V - single grain	1	4	33	0.3
6 V - single grain	0.305	21	56	0.7

3. Results

3.1. Preliminary results: Roughness analyses

An estimation of samples roughness was obtained from AFM scans of the anodized samples surfaces (Table 1). Scan area varied from 200 nm x 200 nm to 10 μm x 10 μm, in order to provide information both on the average surface condition of specimens tested and on single grain roughness. Table 1 reports average surface roughness R_a, maximum peak-to-valley height h_{max}, and the

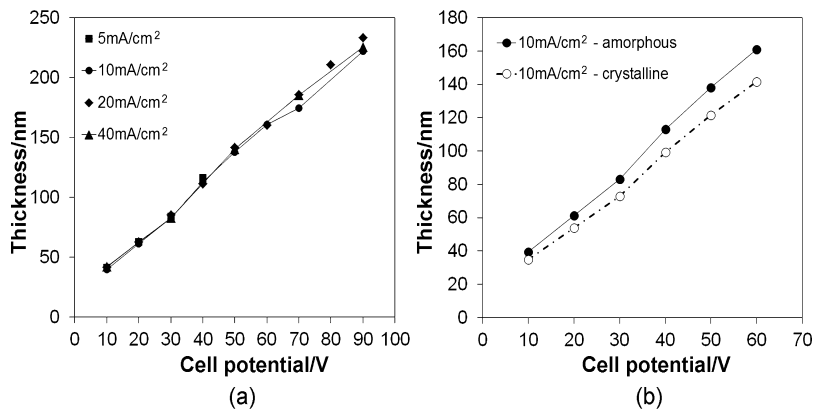

Fig. 1. a) Oxide thickness of specimens anodized with different current density, valid for amorphous oxides; b) thickness obtained by considering the formation of either fully crystalline or fully amorphous oxides.

percent ratio between actual specific surface area and projected area ΔA. In spite of relatively high h_{max} values, the average roughness R_a reached a maximum of 122 nm, with an intra-grain value of few nm. The ratio between specific surface area and projected area was also estimated, and discrepancies never exceeded 6.5%, with an average value < 4%. This parameter was considered of particular relevance in processing coulometric data (see par. 3.3).

3.2. Spectrophotometry

In Fig. 1a, oxide thickness calculated from reflectance spectra is plotted versus applied voltage for specimens anodized in 0.5 M H_2SO_4 with different current densities: data only include oxides produced at 10 V or more, since at lower voltages no interference peak could be measured in the visible range, impeding thickness estimation. For a clearer comparison of curves produced at different current densities, oxides were initially assumed to be amorphous (n_a = 2.2 at 632.8 nm) and possible crystalline phases were not considered at this stage. This approximation holds for specimens anodized at voltage lower than 70 V in galvanostatic conditions at high current density, where the oxide is mostly amorphous, as previously reported [36]; the same condition would not apply to other anodizing conditions, e.g., in presence of a potentiostatic step of cell voltage maintaining once the desired voltage is reached, which would favor oxide crystallization by providing time for structural rearrangements, or in case of lower current density (<5 mA/cm^2) which allows a gradual oxide arrangement already during the anodizing process [37,38].

The maximum mismatch between thicknesses corresponding to crystalline or amorphous oxide structures is shown in Fig. 1b for a sample curve. Tests were only performed on pickled specimens due to the pronounced effect exerted by surface pretreatment on the anodizing ratio, namely, higher anodizing ratio and a more linear trend compared to solely degreased ones, which is symptomatic of a more reliable process [28]. The expected linear oxide thickening with cell voltage was observed–anodizing ratio AR = 2.3 nm/V–coherently with anodizing ratios of pickled titanium described in previous literature works [18–20]. In spite of a good linearity of thickness-voltage dependence, as attested by regression coefficients higher than 0.99, the regression intercept–oxide thickness for V = 0, that is, on pristine titanium specimens before anodizing–was surprisingly high, with a value approaching 20 nm: since specimens were pickled prior to anodizing, this was excluded, as the surface could only present the freshly cancelled and partially rebuilding passive film, whose thickness is expected to lay in the nanometer range (3-5 nm for a fully grown passive film, in this case even lower thickness is expected due to the recent pickling). Therefore, a different anodizing ratio should be expected below 10 V.

3.3. Coulometry

Fig. 2 shows results of coulometric measurements on specimens anodized up to a maximum of 10 V, since at higher voltages oxygen evolution on the anode surface was already discernible, making this method of thickness determination unreliable. Roughness was not taken into account, as its effect is limited to an average 4%, as derived from roughness analyses presented in Table 1. Such quantity was considered negligible for thicknesses calculated by this technique, which never exceeded 45 nm–giving a discrepancy of approximately -1.5 nm on the maximum thickness calculated if roughness is considered, and lower in the other cases. Coulometric data were calculated using two values of TiO_2 density: ρ_a (3.1 g/cm^3) and ρ_c (3.9 g/cm^3) corresponding to amorphous and crystalline oxides with anatase phase, respectively (the latter choice relies on the fact that the first crystal phase generally observed in titanium oxides obtained at increasing cell voltages is anatase, while rutile appears to form at higher voltages [36,39]). Both sets of data are shown for specimens anodized at 10 mA/cm^2, together with the corresponding spectrophotometric thickness measurements.

Concerning the comparison between the two techniques, as expected the best fit with spectrophotometric values is obtained

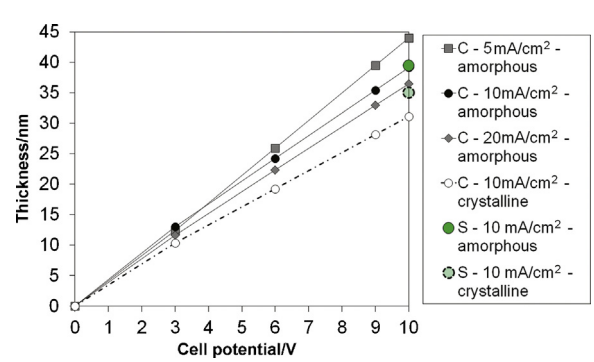

Fig. 2. Oxide thickness–comparison between coulometry (C) and spectrophotometry (S). in the analysis of specimens anodized with 10 mA/cm2, refractive index and density values for both amorphous and crystalline oxides were used.

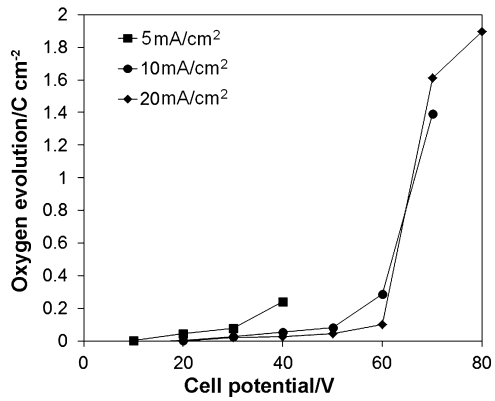

Fig. 3. Amount of current dissipated per unit area in the process as a function of cell voltage, ascribed to the parasitic oxygen evolution reaction.

by using a low density to calculate coulometric data, indicating a prevailingly amorphous nature of thin anodic oxides. In fact, in this way, a mismatch of 1 nm at 10 V is obtained, while if a crystalline structure is considered the mismatch between data provided by the two techniques exceeds 4 nm.

The anodizing ratio calculated below 10 V in such condition (i.e., considering amorphous oxides produced at medium-high current densities, so as to reduce possible crystallization effects and consequent oxygen evolution) is 3.5 ÷ 3.9 nm/V: the higher oxidation kinetics observed below 10 V was ascribed to the poor barrier effect exerted by the growing oxide in its initial phases, assuming that a defective–and possibly porous–oxide is first formed, allowing a faster ionic conduction through the growing layer and therefore a faster oxide growth. Above a few Volts it becomes more difficult for species to cross the oxide and reach the metal-oxide interface as the barrier gets more compact and effective: therefore, the second slope observed in thickness-to-voltage trends decreases to lower values, of approximately 2 nm/V.

On the other hand, it is possible to observe a higher anodizing ratio at lower current densities, which was not noticed in spectrophotometric measurements: this effect was ascribed to the occurrence of parasitic oxygen evolution reactions. More specifically, even at low voltages the application of a low current density may induce the growth of a more orderly structured oxide, enhancing the formation of nanometric crystal domains, which in turn may act as pathways for current leakage and consequently anticipate oxygen evolution [5,18].

This concurrent process decreases anodizing efficiency below 100%: therefore, if the whole current flowing in the circuit is considered, the resulting oxide thickness will be overestimated.

From data shown it was possible to define an agreement between coulometric and spectrophotometric oxide thickness by considering amorphous oxide parameters. Therefore, with the abovementioned exception of specimens anodized at 5 mA/cm^2, it is a good approximation to consider oxygen evolution negligible below 10 V, otherwise a higher thickness would have been inferred by coulometry results.

On the basis of these considerations, we estimated the quantity of current dissipated during the anodizing process of specimens at voltages higher than 10 V: dissipations were ascribed to oxygen evolution, coherently with literature [39–41]. This was done by subtracting to the total circulated charge the charge necessary to build an oxide with thickness equal to that provided by spectrophotometry for amorphous oxides, which was taken as reference for this estimation. Results are presented in Fig. 3. It is possible to observe how, at low voltages, the amount of oxygen produced per unit area is similar for all current densities considered; moreover, below 40 V the ratio between dissipated current and duration of the test–i.e., time allowed for oxygen to develop–is similar, in the order of 5-15 C/cm^2·h, which indicates similar leakages in all anodic oxides at any voltage per unit time. This was ascribed to the similarities in oxide structure, with few weak points–nanocrystals–that allow current leakage, and therefore oxygen development, in similar quantity. On the other hand, above 50 V discrepancies grow, and dissipations increase with cell voltage in a steeper way, reaching first tens, then hundreds of C/cm^2·h. The substantial crystallization of the oxide, which is also observed with traditional techniques (XRD, Raman spectroscopy), can account for this effect [5,36]. Interestingly, the voltage threshold above which this change in behavior is observed decreases with decreasing anodizing current density: this is in agreement with the fact that lower current densities allow a better arrangement of the oxide during its growth, promoting its crystallization at lower voltages.

3.4. C-AFM imaging

As previously mentioned, oxide structure was investigated by C-AFM, in order to spot possible heterogeneities in the structure or thickness of anodic oxides produced.

Experimental tests aimed at probing first the heterogeneities leading to high current leakage, and for that only the C-AFM images obtained by the gain 1 MΩ were considered.

Results showed the presence of areas with high conductance (current ∼ μA) and areas with lower conductance (current < 10 nA), as shown in Fig. 4 for specimens anodized at 3 V, 6 V and 9 V.

It is important to note that non-anodized titanium morphology is textured with clearly visible grain boundaries (figure not shown); therefore, a different oxide growth–both in terms of thickness and structure–at grain boundaries can be expected owing to different reactivity, on account of metallurgical impurities and heterogeneities [42].

Therefore, heterogeneities in conductance were first ascribed to differential oxide growth kinetics, since a delayed growth was observed mainly on titanium grain boundaries, as can be evinced by comparing height and current profiles of the same area: this can be ascribed to an island-like initial growth of the oxide. A full coverage of the surface with good oxide homogeneity was only reached above 9-10 V of cell voltage, which is in agreement with abovementioned changes in oxidation kinetics (coulometry and spectrophotometry measurements).

It is important to emphasize that few nanometers of thickness variation can induces large variations of measured current, even by several orders of magnitudes, owing to the highly non-linear current-to-voltage characteristic; this can be fitted by using field emission tunneling formulation, as reported in previous works [43,22]. In addition to this factor, high conductance regions may correspond as well to higher oxide defectiveness arising from the corresponding structural and chemical defectiveness of substrate grain boundaries compared to bulk grain structure, for instance to the formation of substoichiometric oxides with the presence of Ti^{2+} and Ti^{3+} [45]. Given their superior conductance, titanium grain boundaries should also be considered as preferential spots for oxygen evolution reactions [46].

Another interesting feature of oxides conductance arises if low range current analyses are considered (Fig. 5). This can be done by using the second gain of 1 GΩ of the ORCA module, that is, by increasing current sensitivity [47]. Fig. 5 shows the AFM topography scan and corresponding deflection and current images obtained with the 1 MΩ and 1 GΩ gain resistance. For clarity, only measurements of the oxide anodized at 6 V are shown; similar results and conclusions were obtained on other specimens.

The deflection scan reveals the oxide nanostructure and mainly the grain boundaries of the underlying titanium substrate. In

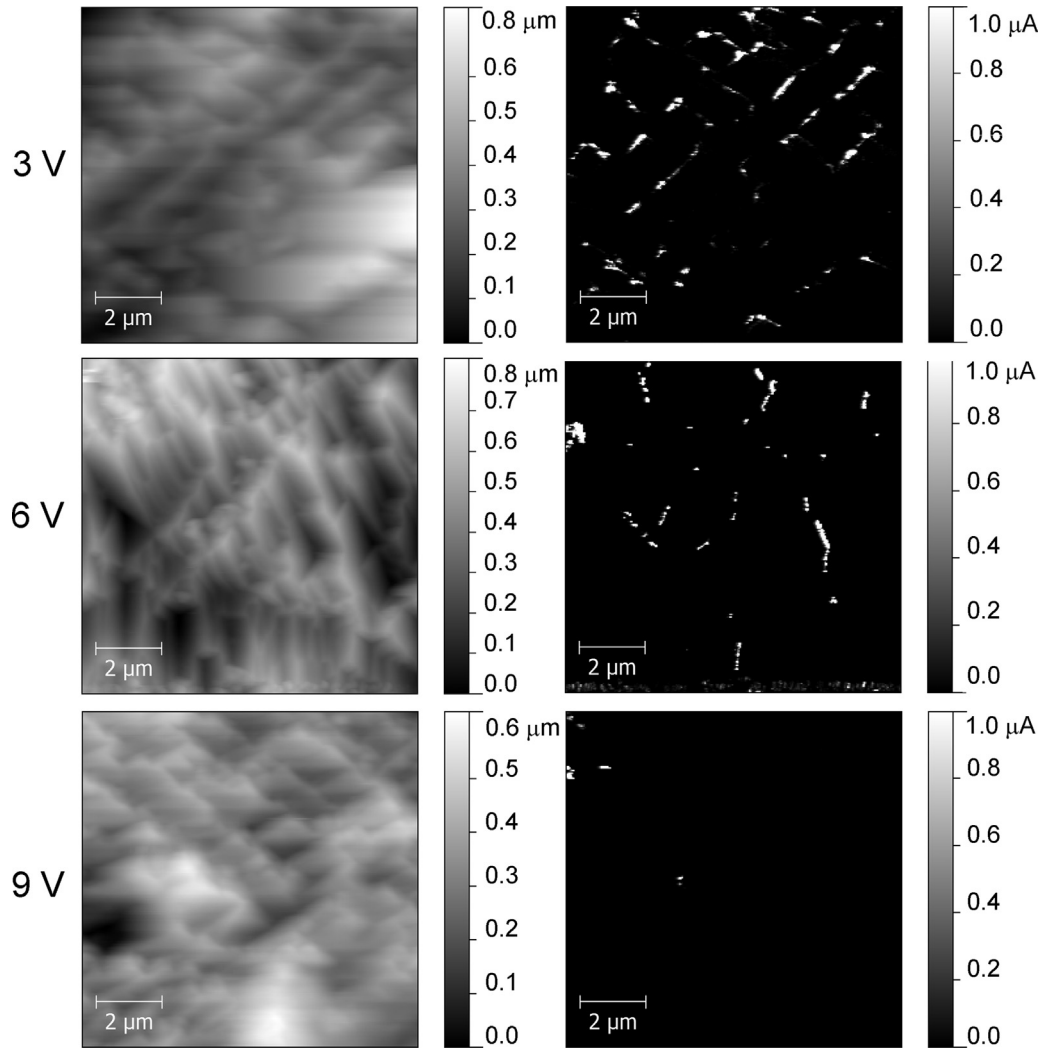

Fig. 4. Height (left) and current (right) images on a10 μm area of oxides produced at 3 V, 6 V and 9 V. Data acquired at surface voltage of 1 V, 2 V, and 1.5 V, respectively.

addition to the highly conductive spots (and lines) that mainly correspond to grain boundaries–areas with high defectiveness and/or low oxide thickness, as previously mentioned), it is possible to evidence the presence of other conductive spots inside grains (Fig. 5d). This proves the presence of local variation and heterogeneities unrelated to oxide thickness, which is supposed to be uniform within such a homogeneous area as a single titanium grain is–also considering the extremely low roughness of such area, of the order of few nm (Table 1).

This was then ascribed to local changes in oxide structure, which could be responsible for this alteration of conductance, and in particular to a possible nucleation of crystallites within the oxide: this hypothesis was supported by analyses performed on the surface of specimens anodized at 20 V and more, where extensive oxygen development was observed during oxidation, and where an increase in nanosized conductive spots within grains was observed. Similar results were obtained by C-AFM imaging on silicon thin films where nanosize crystalline domains appear more conductive than the insulating amorphous matrix [24]. The presence of crystal phases could not be observed by XRD analyses, due to the small size of the domains observed.

In order to reveal the presence of nanocrystallites and their evolution with cell voltage, high resolution C-AFM images were recorded, by using 1 GΩ gain resistance, on all samples with cell voltage ranging from 3 V up to 20 V (Fig. 6). Neglecting the aforementioned grain boundary effects (particularly visible at cell voltage of 3 V and 6 V), conductive spots resulted to increase in size and number with anodizing voltage from few tens of nanometers to some hundreds of nanometers, with collected current values in the range of hundreds of pA to few nA.

3.5. *I-V spectroscopy*

In order to get deep insight on the electrical behavior of anodic TiO_2, point current-to-voltage spectroscopy was employed by applying a cyclic bias to the anodized titanium sample. These analyses carried out at different surface sites pointed out the n-type semiconductivity characteristic of anodic titanium oxides at the conductive domains, with current flowing preferentially in forward bias (negative specimen bias), thus confirming the formation of a Schottky barrier between metal (AFM tip) and n-type semiconductor (oxide).

At high positive voltage (> 3 V), a sharp current increase was observed and attributed to the breakdown voltage of the oxide (results not shown). The breakdown mechanism and its relation with oxide thickness and growth kinetics are not discussed in the present paper.

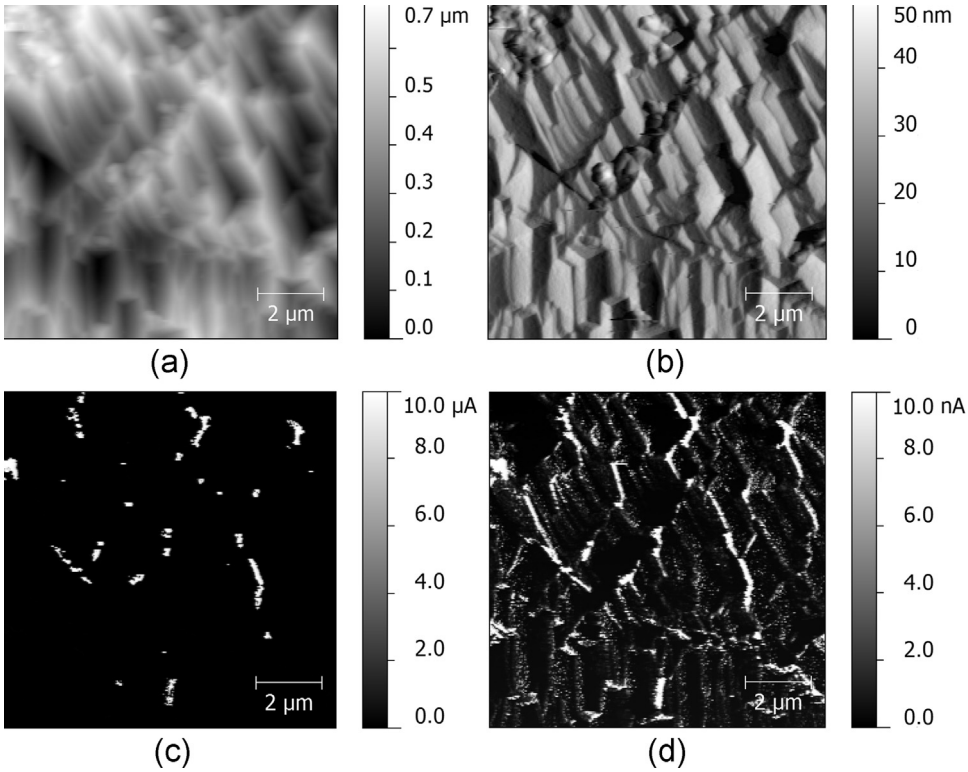

Fig. 5. a) Height, b) deflection and corresponding current images with c) 1 MΩ gain resistance and d) 1 GΩ gain resistance of sample anodized at 6 V cell voltage. Data acquired with surface voltage of 4 V.

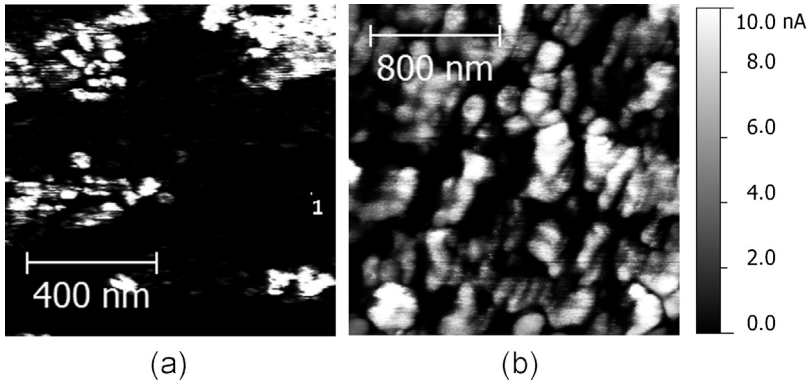

Fig. 6. High magnification C-AFM current images on TiO_2 grown a different cell voltage: a) 9 V, b) 20 V, revealing the conductive spots corresponding to nanocrystallites in the insulating amorphous matrix. Data acquired with surface voltage of a) 4 V and b) 3 V. Crystals size increases with cell voltage.

The formulated hypothesis of a nanocrystalline texture in a prevalently amorphous oxide was further investigated by performing higher magnification scans as well as local I-V curves at different areas both on conductive spots and on the insulating amorphous matrix (Fig. 7).

In line with C-AFM imaging qualitative description, I-V spectroscopy showed the enhanced conductance of nanocrystals as current increased to few nA by applying a voltage of -2 V. In contrast, amorphous TiO_2 showed an insulating behavior and no current could be measured even by applying high negative voltage of -6 V.

Finally, low voltage oxides (3 to 9 V) were characterized with I-V module of C-AFM by sweeping the specimen bias from 3 V to -4 V and back to 3 V. Fig. 8 shows the resulting curves for a specimen anodized at 6 V, tested both on highly conductive regions that reached the range of µA–which were assumed to correspond to highly defective and thinner oxide regions at titanium

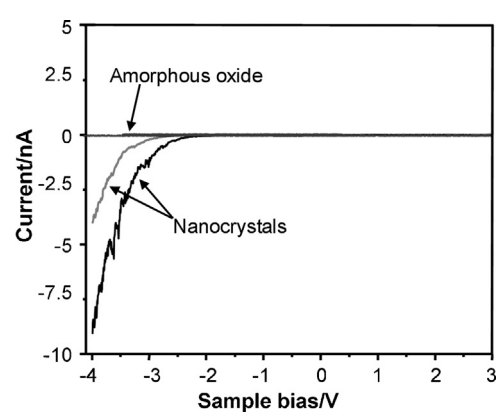

Fig. 7. I-V curves recorded in areas of the oxide showing different conductivity (bias applied to the sample).

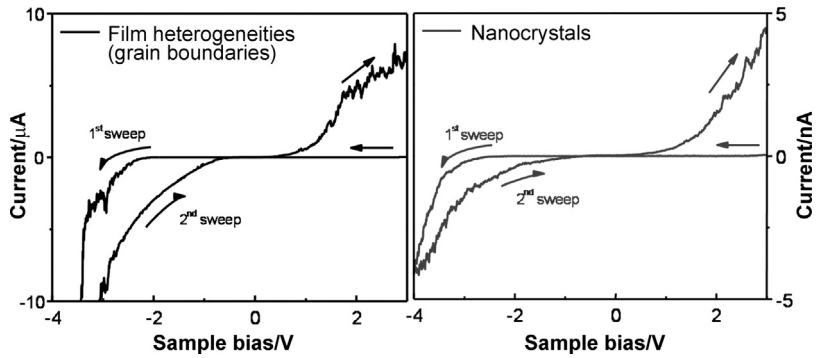

Fig. 8. Memristive switching curves recorded on a 6 V (25 nm) anodic oxide: measurements performed on grain boundary regions with higher conductivity (left) and on nanocrystals (right).

grain boundaries–and on local conductive spots (nA)–which were previously indicated as possible nanocrystalline regions. The amorphous matrix was not included, given the absence of conductance (Fig. 7). In both conductive areas the behavior observed was a bias-dependent bipolar switching, indicative of memristive characteristics: similar results were obtained in previous literature works by using a micro-probe technique [12]. Analogous switching resistance behavior was also observed on specimens anodized with cell voltage of 3 V and 9 V. This effect could be ascribed to non-stoichiometric oxide areas, according to literature studies, which identified the presence of Magnéli phases as responsible for memristive behavior [48].

Further analyses of the effect of cell voltage and resulting TiO_2 structure on its electric properties are needed to gain a deeper insight of the switching mechanism involved in these anodic oxides, with particular reference to the role of stoichiometry defects (oxygen vacancies) in crystalline domains at the Ti/TiO_2 interface.

4. Discussion

Data presented in the previous paragraph shed a new insight onto the characteristics of anodic titanium oxides produced in acid electrolytes, with particular reference to diluted sulfuric acid, which is one of the most commonly utilized anodizing baths. Such findings deserve to be briefly summarized.

Oxide growth was observed to show two trends: a first, more rapid increase when cell voltage is limited to few Volts (anodizing ratio between 3.5 and 4 nm/V), and a slower phase above approximately 10 V (anodizing ratio 2.3 nm/V). The coincidence of this transition with the conjunction point of the two techniques applied is a critic aspect, which doesn't allow a clear confirmation of the finding. Yet, some considerations support the validity of this behavior:

- A different trend in growth rate was expected below 10 V: in fact, the extrapolation of spectrophotometric data at V = 0 indicated a native oxide thickness of 18 nm (from linear interpolation of experimental data: $\delta = 2.3\ \text{nm/V} \cdot \Delta V + 18\ \text{nm}$, where δ is oxide thickness and ΔV is cell voltage). Specimens were freshly pickled: therefore, although a passive film may be forming, it is unlikely to be thicker than few nm, with minor influence on the anodizing ratio.
- To process coulometric results, O_2 evolution was considered negligible below 10 V. This assumption is supported by the correspondence found between coulometry and spectrophotometry in the overlapping point of the two techniques. Moreover, a visual observation couldn't detect any oxygen bubble forming on the specimen surface, while bubbling was clearly observed at higher voltages: this doesn't exclude a partial current leakage and consequent O_2 evolution, but reinforces the hypothesis that process efficiency would be only marginally affected. Given the small thickness of oxides considered, it is important to consider that even a 10% drop in efficiency would cause oxide thickness to be overestimated only by 10%, that is, 5 nm. Such drop was actually observed at 20 V of cell tension, with respect to the actual oxide thickness measured by spectrophotometry, therefore at lower voltages–including the case considered–the drop is expected to be lower, consistently with the trend observed of increasing dissipations with increasing voltage.
- Only the careful choice of relevant parameters–i.e., oxide refractive index and density–allows to obtain consistent data from coulometry and spectrophotometry. The data obtained from the two techniques only match when considering completely–or prevalently–amorphous TiO_2, in agreement with our assumptions.

Finally, as proven by oxygen evolution data, below 40 V the current dissipated per unit time is almost constant at all cell voltages reached and current densities applied, indicating the formation of a similar oxide structure. Conversely, dissipations increase above a threshold–40 V at 5 mA/cm^2, 60 V at 10 mA/cm^2, 70 V at 20 mA/cm^2–which is related to the first observation of a sensible crystalline component, as shown in previous works [5,36]. This sharp threshold further confirms the predominantly amorphous nature of low voltage oxides, also proven by C-AFM analyses, with local formation of nanocrystals that account for oxygen evolution and for the development of a memristive behavior, while the production of detectable crystalline domains is only observed at higher voltages.

5. Conclusions

The work presented investigated the nanoscale structure and thickness of titanium oxides resulting from anodizing titanium in diluted sulfuric acid. Findings highlighted a multifaceted heterogeneous nature of anodic oxides, whose thickness increases linearly with cell voltage, with a prevalently amorphous structure and the formation of nanocrystals that increase in number and size with increasing voltage. Moreover, the system tip/nanocrystals/Ti presents a resistance switching at successive voltage sweeps which is characteristic of a memristive behavior. A similar characteristic is observed in thin oxide films produced by cell voltages from 3 V to 9 V. A fine tuning of oxide electrical properties is therefore possible by modulating anodizing parameters and cross-checking the obtained characteristics through the non-destructive techniques proposed.

References

[1] M. Vishwas, S.K. Sharma, N. Rao, S. Mohan, K.V. Arjuna Gowda, R.P.S. Chakradhar, Sol-gel synthesis, characterization and optical properties of TiO_2 thin films deposited on ito/glass substrates, Mod. Phys. Lett. B 24 (2010) 807.

[2] L. Tran, T. Tuan, C.N. Huu, N.S.L. Dac, N.H. Minh, Q.N. Dihn, Fabrication and Characterization of Multi-layer Heat Mirror with Photocatalytic Properties, Chi. Phys. Lett. 26 (2009) 116801.

[3] S. Ito, T. Takeuchi, T. Katayama, M. Sugiyama, M. Matsuda, T. Kitamura, Y. Wada, S. Yanagida, Conductive and transparent multilayer films for low-temperature-sintered mesoporous TiO_2 electrodes of dye-sensitized solar cells, Chem. Mater. 15 (2003) 2824–2828.

[4] S. Jung, J. Kong, S. Song, K. Lee, T. Lee, H. Hwang, S. Jeon, Resistive switching characteristics of solution-processed TiO_x for next-generation non-volatile memory application; transparency, flexibility, and nano-scale memory feasibility, Microelectron. Eng. 88 (2011) 1143–1147.

[5] M.V. Diamanti, B. Del Curto, M.P. Pedeferri, Anodic oxidation of titanium: from technical aspects to biomedical applications, J. Appl. Biomater. Biomech. 9 (2011) 55–69.

[6] J.F. Vanhumbeeck, J. Proost, Current understanding of Ti anodization, Corros. Rev. 27 (2009) 117–194.

[7] F.C. Walsh, C.T.J. Low, R.J.K. Wood, K.T. Stevens, J. Archer, A.R. Poeton, A. Ryder, Plasma electrolytic oxidation (PEO) for production of anodised coatings on lightweight metal (Al, Mg, Ti) alloys, Trans. Inst. Metal Finishing 87 (2009) 122–135.

[8] D.B. Strukov, G.S. Snider, D.R. Stewart, R.S. Williams, The missing memristor found, Nature 453 (2008) 80–84.

[9] A. Thomas, Memristor-based neural networks, J. Phys. D 46 (2013) 093001.

[10] B.J. Choi, D.S. Jeong, S.K. Kim, C. Rohde, S. Choi, J.G. Oh, H.J. Kim, C.S. Hwang, K. Szot, R. Waser, B. Reichenberg, S. Tiedke, Resistive switching mechanism of TiO2 thin films grown by atomic-layer deposition, J. Appl. Phys. 98 (2005) 1–10.

[11] L. Chua, The missing circuit element, IEEE Trans. Circuit Theory 18 (1971) 507–519.

[12] K. Miller, K.S. Nalwa, A. Bergerud, N.M. Neihart, S. Chaudhary, Memristive behavior in thin anodic titania, IEEE Electron. Device Lett. 31 (2010) 737–739.

[13] J.E. Yoo, K. Lee, A. Tighineanu, P. Schmuki, Highly ordered TiO_2 nanotube-stumps with memristive response, Electrochem. Commun. 34 (2013) 177–180.

[14] Q. Liu, S. Long, H. Lv, W. Wang, J. Niu, Z. Huo, J. Chen, M. Liu, Controllable growth of nanoscale conductive filaments in solid-electrolyte-based ReRAM by using a metal nanocrystal covered bottom electrode, ACS Nano 4 (2010) 6162–6168.

[15] D.H. Kwon, K.M. Kim, J.H. Jang, J.M. Jeon, M.H. Lee, G.H. Kim, X.S. Li, G.S. Park, B. Lee, S. Han, M. Kim, C.S. Hwang, Atomic structure of conducting nanofilaments in TiO_2 resistive switching memory, Nat. Nanotechnol. 5 (2010) 148–153.

[16] R. Muenstermann, T. Menke, R. Dittmann, R. Waser, Coexistence of filamentary and homogeneous resistive switching in Fe-Doped $SrTiO_3$ thin-film memristive devices, Adv. Mater. 22 (2010) 4819–4822.

[17] Y. Hu, D. Perello, M. Yun, D-H. Kwon, M. Kim, Variation of switching mechanism in TiO_2 thin film resistive random access memory with Ag and graphene electrodes, Microelectron. Eng. 104 (2013) 42–47.

[18] U.R. Evans, The colors due to thin films on metals, Proc. Roy. Soc. Lond. Ser. A 107 (1925) 228–237.

[19] S. Van Gils, P. Mast, E. Stijns, H. Terryn, Colour properties of barrier anodic oxide films on aluminium and titanium studied with total reflectance and spectroscopic ellipsometry, Surf. Coat. Techol. 185 (2004) 303–310.

[20] M.V. Diamanti, S. Aliverti, M.P. Pedeferri, Decoupling the dual source of colour alteration of architectural titanium: Soiling or oxidation? Corros. Sci. 72 (2013) 125–132.

[21] S. Schroth, M. Schneider, T. Mayer-Uhma, A. Michaelis, V. Klemm, Investigation of thin oxide films on titanium for capacitor applications, Surf. Interf. Anal. 40 (2008) 850–852.

[22] W. Frammelsberger, G. Benstetter, J. Kiely, R. Stamp, C-AFM-based thickness determination of thin and ultra-thin SiO_2 films by use of different conductive-coated probe tips, Appl. Surf. Sci. 253 (2007) 3615–3626.

[23] T. Souier, F. Martin, C. Bataillon, J. Cousty, Local electrical characteristics of passive films formed on stainless steel surfaces by current sensing atomic force microscopy, Appl. Surf. Sci. 256 (2010) 2434–2439.

[24] B. Rezek, J. Stuchlık, A. Fejfar, J. Kocka, Local characterization of electronic transport in microcrystalline silicon thin films with submicron resolution, Appl. Phys. Lett. 74 (1999) 1475–1477.

[25] C. Moreno, C. Munuera, X. Obradors, C. Ocal, The memory effect of nanoscale memristors investigated by conducting scanning probe microscopy methods, Beilstein J. Nanotechnol. 3 (2012) 722–730.

[26] T.S. Herng, A. Kumar, C.S. Ong, Y.P. Feng, Y.H. Lu, K.Y. Zeng, J. Ding, Investigation of the non-volatile resistance change in noncentrosymmetric compounds, Sci Rep. 2 (2012) 587.

[27] Y. Du, A. Kumar, H. Pan, K. Zeng, S. Wang, P. Yang, A.T.S. Wee, The resistive switching in TiO_2 films studied by conductive atomic force microscopy and Kelvin probe force microscopy, AIP Advances 3 (2013) 082107.

[28] M.V. Diamanti, B. Del Curto, V. Masconale, C. Passaro, M.P. Pedeferri, Anodic coloring of titanium and its alloy for jewels production, Color Res. Appl. 37 (2012) 384–390.

[29] Z. Xia, H. Nanjo, H. Tetsuka, T. Ebina, M. Izumisawa, M. Fujimura, J. Onagawa, Crystallization of the anodic oxide on titanium in sulphuric acids solution at a very low potential, Electrochem. Commun. 9 (2007) 850–856.

[30] M. Zhang, G. Lin, C. Dong, L. Wen, Amorphous TiO_2 films with high refractive index deposited by pulsed bias arc ion plating, Surf. Coat. Technol. 201 (2007) 7252–7258.

[31] A. Alkhatib, T. Souier, M. Chiesa, Morphology dependent electrical transport behavior in gold nanostructures, Thin Solid Films 520 (2011) 656–661.

[32] S. Santos, L. Guang, T. Souier, K. Gadelrab, M. Chiesa, N.H. Thomson, A method to provide rapid in situ determination of tip radius in dynamic atomic force microscopy, Review of Scientific Instruments 83 (2012) 043707.

[33] T. Souier, M. Chiesa, Effect of surface conditions and strain hardening on the passivity breakdown of 304 stainless steel, J. Mater. Res. 27 (2012) 1580–1588.

[34] D. Nečas, P. Klapetek, Gwyddion: an open-source software for SPM data analysis, Cent. Eur. J. Phys. 10 (2012) 181–188.

[35] I. Horcas, R. Fernández, J.M. Gómez-Rodríguez, J. Colchero, J. Gómez-Herrero, A.M. Baro, A software for scanning probe microscopy and a tool for nanotechnology, Rev. Sci. Instrum. 78 (2007) 013705.

[36] M.V. Diamanti, M.P. Pedeferri, Effect of anodic oxidation parameters on the titanium oxides formation, Corros. Sci. 49 (2007) 939–948.

[37] B. Davepon, J.W. Schultze, U. König, C. Rosenkranz, Crystallographic orientation of single grains of polycrystalline titanium and their influence on electrochemical processes, Surf. Coat. Technol. 169-170 (2003) 85–90.

[38] A. Aladjem, Anodic oxidation of titanium and its alloys, J. Mater. Sci. 8 (1973) 688–704.

[39] H. Habazaki, M. Uozumi, H. Konno, K. Shimizu, P. Skeldon, G.E. Thompson, Crystallization of anodic titania on titanium and its alloys, Corros. Sci. 45 (2003) 2063–2073.

[40] J.-L. Delplancke, R. Winand, Galvanostatic anodization of titanium–II. Reactions efficiencies and electrochemical behaviour model, Electrochim. Acta 33 (1988) 1551–1559.

[41] Y.-T. Sul, C.B. Johansson, Y. Jeong, T. Albrektsson, The electrochemical oxide growth behaviour on titanium in acid and alkaline electrolytes, Med. Eng. Phys. 23 (2001) 329–346.

[42] F. Ren, L. Huang, Y. Ling, J. Feng, Grain boundaries dependent hydrogen sensitivity in MAO-TiO_2 thin films sensors, Sens. Actuators B 148 (2010) 195–199.

[43] T. Souier, C. Maragliano, M. Stefancich, M. Chiesa, How to achieve high electrical conductivity in aligned carbon nanotube polymer composites, Carbon 64 (2013) 150–157.

[45] S. Kumar, T.S.N.S. Narayanan, S.G.S. Raman, S.K. Seshadri, Thermal oxidation of CP-Ti: Evaluation of characteristics and corrosion resistance as a function of treatment time, Mater. Sci. Eng. C 29 (2009) 1942–1949.

[46] X. Yin, Y. Wang, B. Liu, X.B. Luo, Effects of the grain boundary on phase structure and surface morphology of TiO_2 films prepared by MAO technology, Surf. Interface Anal. 44 (2012) 276–281.

[47] T. Souier, G. Li, S. Santos, M. Stefancich, M. Chiesa, Conductive scanning probe microscopy of nanostructured Bi_2Te_3, Nanoscale 4 (2012) 600–606.

[48] K.M. Kim, G.H. Kim, S.J. Song, J.Y. Seok, M.H. Lee, J.H. Yoon, C.S. Hwang, Electrically configurable electroforming and bipolar resistive switching in Pt/TiO_2/Pt structures, Nanotechnology 21 (2010) 305203.